Proceedings of the 20th National Conference on Superconductivity "New Phases, Concepts and Advances"

Hubbard Subbands and Superconductivity in the Infinite-Layer Nickelate

T. Plienbumrung[a,b], M. Daghofer[a,b], M.T. Schmid[c] and A.M. Oleś[e,d,*]

[a] *Institute for Functional Matter and Quantum Technologies, University of Stuttgart, Pfaffenwaldring 57, D-70550 Stuttgart, Germany*
[b] *Center for Integrated Quantum Science and Technology, University of Stuttgart, Pfaffenwaldring 57, D-70550 Stuttgart, Germany*
[c] *Waseda Research Institute for Science and Engineering, Waseda University, Okubo, Shinjuku, Tokyo, 169-8555, Japan*
[d] *Max Planck Institute for Solid State Research, Heisenbergstr. 1, D-70569 Stuttgart, Germany*
[e] *Institute of Theoretical Physics, Jagiellonian University, Profesora Stanisława Łojasiewicza 11, PL-30348 Kraków, Poland*

Doi: 10.12693/APhysPolA.143.200 *e-mail: a.m.oles@fkf.mpi.de

An effective two-dimensional two-band model for infinite-layer nickelates consists of bands obtained from $d_{x^2-y^2}$ and s-like orbitals. We investigate whether it could be mapped onto a single-band Hubbard model and the filling of Hubbard bands. We find that both one-band physics and a Kondo-lattice regime emerge from the same two-orbital model, depending on the strength of electronic correlations and the filling of the itinerant s-band. Next, we investigate one-particle excitations by changing the screening. First, for weak screening, the strong correlations push electrons out of the s-band so that the undoped nickelate is similar to a cuprate. Second, for strong screening, the s and $d_{x^2-y^2}$ bands are both partly filled and weakly coupled. Particularly in this latter regime, mapping to a one-band model gives significant spectral weight transfer between the Hubbard subbands. Finally, we show how the symmetry of superconducting phases depends on the interaction parameters and determine the regions of d-wave or s-wave symmetry.

topics: Hubbard model, superconductivity, infinite-layer nickelate

1. Introduction

A few years ago, superconductivity was reported in infinite-layer $NdNiO_2$ thin films with Sr doping [1]. The lattice structure shares similarities with cuprate superconductors, with NiO_2 planes taking the place of CuO_2 planes. While both can be expected to be quite correlated and both show antiferromagnetic (AFM) superexchange [2–6], there are some microscopic differences. One is the lack of apical oxygens in the Ni case, which affects crystal-field energies, the other is the presence of dispersive rare-earth states close to the Fermi level. Whether one starts from isolated NiO_2 layers [2–8] or from band-structure calculations [9–16], one expects that more than one orbital or band might be relevant.

While single-band [17] and three-band [11, 18] models have also been proposed, two bands cross the Fermi level (see Fig. 1), and many groups have accordingly investigated two-band models [18–23]. One of the bands has a large contribution from the $x^2 - y^2$ orbital at Ni, and its dispersion is nearly perfectly two-dimensional (2D). This band can be expected to share features with the Cu-dominated band of the cuprates and to be rather correlated. In the second band, rare-earth states hybridize with Ni apical states, thus obtaining some Ni($d_{3z^2-r^2}$) and Ni(d_{xy}) character, however, its wave function has s-symmetry [20], and we denote it accordingly. Previous studies of various two-band models have yielded a large variety of potential pairing symmetries [7, 24], among them s, d, and $s_\pm$-wave states [8, 11, 18], while a one-band scenario favors d-wave [17].

The s-like band lies mostly above the Fermi level, however, it forms electron pockets around the Γ and A points in the Brillouin zone. In the density functional theory (DFT) band structure, the pockets account for ≈ 7% of the occupied states [25]. Even without Sr-doping, these electrons are thus

missing from the $x^2 - y^2$ band. When translating to a cuprate scenario, it should be noted that 5% of Sr doping suffices to destroy antiferromagnetism in La_2CuO_{4-y} [26]. We thus have to expect partly filled bands, and at least one of them is correlated.

The purpose of this paper is to investigate the evolution of the bands shown in Fig. 1 with crystal-field splittings and electron correlations in both bands. Thereby we investigate to what extent multi-band effects come into play in nickelates. It is important to realize that partial filling of the strongly correlated x^2-y^2 orbitals means that the electronic spectral weight may be transferred from the upper Hubbard band (UHB) to the lower Hubbard band (LHB) above the Fermi energy. The mechanism of such a weight transfer is well known for the doped Hubbard model [27, 28]. Another mechanism that promotes such a weight transfer is interaction screening, which generates finite filling within the weakly correlated orbitals of s-wave symmetry. It is remarkable that for both very weak and strong screening, the bands mostly decouple, and the effective physics becomes similar to a single Hubbard band [17]. We then find a Mott insulator (a doped band with potential d-wave pairing) for strong (weak) correlations. Correlation strength thus emerges as an important factor in the description of nickelate superconductors.

The rest of this paper is organized as follows. The two-band model arises from the electronic structure calculations as described in Sect. 2.1. Electronic interactions are given by two Kanamori parameters for an atom α, $\{U_\alpha, J_H\}$, and we discuss their screening in Sect. 2.2. Next, in Sect. 3.1, we investigate a very wide range of potential regimes going from weak to very strong correlations. Then we show how the density of states changes with screening for strong and weak interactions in Sect. 3.2. Finally, we present the essential AFM and superconducting (SC) phases for various regimes of screening in Sect. 3.3. The paper is concluded in Sect. 4.

2. Two-band model and methods

2.1. Kinetic energy

We start with the kinetic energy in the electronic structure. The DFT band structure (see Fig. 1) is calculated with the QUANTUM ESPRESSO code [29–31] using a plane-wave pseudopotential method [32]. As discussed in [33], many models can be constructed that differ in the shape of the apical s-like orbital. Since their hopping integrals, given in [33], are nevertheless very similar, the kinetic energy is not affected by this ambiguity in any physically relevant way.

The Wannier90 interface [34] gives the parametrization,

$$H_{\rm kin} = \sum_{i,\lambda=d,s;\sigma} \epsilon_\lambda d^\dagger_{i\lambda\sigma} d_{i\lambda\sigma} + \sum_{ij,\{\lambda\mu\},\sigma} t^{\lambda\mu}_{ij} d^\dagger_{i\lambda\sigma} d_{j\mu\sigma}, \tag{1}$$

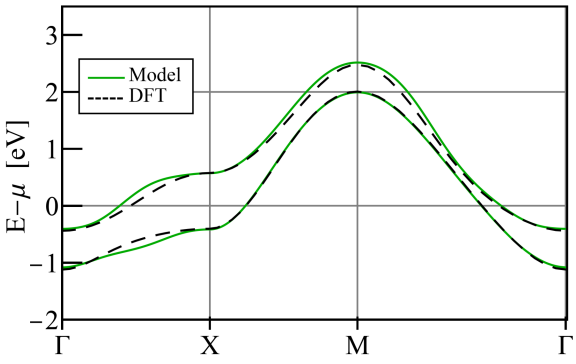

Fig. 1. Non-interacting band structure of $NdNiO_2$: DFT bands crossing the Fermi surface (black dashed lines) and the 2D tight-binding model obtained by projecting a Wannier fit onto the plane along 2D path (green solid lines). The Fermi energy $E = \mu$ corresponds to the DFT electronic structure.

where $d_{i\lambda\sigma}$ ($d^\dagger_{i\lambda\sigma}$) annihilates (creates) an electron at site i in orbital $\lambda = d, s$, with spin σ (d and s refer to the two bands discussed above and shown in Fig. 1). Hopping parameters $t^{\lambda\mu}_{ij}$ and on-site energies ϵ_λ are given in [33]. We project these three-dimensional bands onto the (x, y)-plane, as we are here mostly interested in the correlated $x^2 - y^2$ states, whose band is already quite 2D to start with [33].

2.2. Interactions and screening effect

While the rather extended wave-function of (especially) the s-like state might lead to longer-ranged Coulomb interactions, on-site terms can be expected to dominate, and we use (intraorbital and interorbital) Coulomb elements of the form [3],

$$\begin{aligned} H_{\rm int} = & \sum_{i,\lambda=d,s} U_\lambda n_{i\lambda\uparrow} n_{i\lambda\downarrow} + \left(U' - \frac{J_H}{2}\right) \sum_i n_{id} n_{is} \\ & - 2J_H \sum_i \boldsymbol{S}_{id} \cdot \boldsymbol{S}_{is} \\ & + J_H \sum_i \left(d^\dagger_{id\uparrow} d_{id\downarrow} d^\dagger_{is\downarrow} d_{is\uparrow} + \text{h.c.} \right), \end{aligned} \tag{2}$$

where $n_{i\lambda\sigma}$ is the electron number operator at site i, in orbital λ and for spin σ and $\{\vec{S}_{i\lambda}\}$ the corresponding spin operator. Intraorbital Coulomb repulsion U_λ depends on the band index $\lambda = d, s$. Hund's exchange is given by J_H, and interorbital repulsion U' couples the bands.

Upper limits for the 'bare' U_d and J_0 are given by their atomic values $U_d \approx 8$ eV and $J_0 \approx 1.2$ eV, as one might use in modeling an insulating NiO_2 layer [2, 3]. However, when projecting out oxygen states and using the Wannier functions instead, the effective values have to be significantly reduced. In the case of U_s, atomic values for Ni cannot be even taken as a starting point, as the s-orbital is mostly

made up of rare-earth states and is not centered on a Ni site [20]. The strong Nd($5d$) character and very itinerant character of the s-bands suggest that their effective interaction should be strongly screened, in fact, less screening can be expected for the d states. One thus expects $U_d > U_s$, which we take into account in a phenomenological way via a screening parameter $\alpha \in [0, 1]$, so that

$$U_s = \alpha U_d, \quad J_H = \alpha J_0, \quad U' = U_s - 2J_H. \quad (3)$$

This parametrization provides the simplest approach to discuss the interplay of a more and a less correlated band.

We then use the Lanczos exact diagonalization to treat the full Hamiltonian $H = H_{\rm kin} + H_{\rm int}$ on an eight-site square cluster standing for a NiO_2 plane. Orbital densities are analyzed following [33] for the two orbitals, d and s. Below, we summarize the evolution of the density of states in the correlated d band and the accompanying s band. We particularly focus on the circumstances favoring the electron transfer between the Hubbard subbands in the correlated band.

3. Numerical results

3.1. Hubbard subbands

To understand the occurrence of possible SC phase in infinite-layer nickelates, we consider first the one-particle spectra in the normal phase. Figure 2 shows the orbital-resolved density of states, taking two values of the Coulomb interaction $U_d = 8.0$ and 4.0 eV. The larger value is the same as interactions in cuprates [35] and could be considered the upper limit; the lower value stands for effective Coulomb interactions in the metallic state in nickelates, where Coulomb interactions are weaker. Here, we begin with unscreened interactions in the s band, i.e., we take $\alpha = 1.0$.

In both cases of large $U_d = 8.0$ eV and moderate $U_d = 4.0$ eV, one finds a Mott insulator with two subbands separated by a gap, the occupied LHB and the empty UHB. For large $U_d = 8.0$ eV, the gap s ≈ 3.5 eV, and the Fermi energy falls within the gap (see Fig. 2a). This may be considered a textbook example of a Mott insulator. Then one also finds an AFM order in LHB.

When $U_d = 4$ eV, the gap in the correlated band decreases to less than ≈ 1.0 eV, and the tail of the s band falls below the Fermi energy, which still separates the occupied and unoccupied states of LHB (see Fig. 2b). However, we should keep in mind that the calculations are done for a finite system, and we cannot exclude a metallic phase in the thermodynamic limit. In any case, one finds a small fraction of electrons occupying the s states, and these states are just below the Fermi energy (see Fig. 2b). Here, the correlated LHB band is less than half-filled and develops dynamics. As a result, electron transfer from UHB to the unoccupied part of LHB increases, and the total occupancy of LHB exceeds 0.5. We

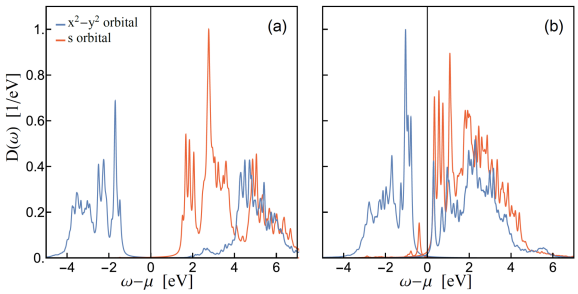

Fig. 2. Density of states $D(\omega)$ of undoped nickelate with unscreened interactions ($\alpha = 1$). Fermi energy is set to zero; the orbital densities are normalized to one (per spin). Intraorbital Coulomb interaction in (2) is selected at (a) $U_d = 8$ eV and (b) $U_d = 4$ eV.

conclude that the presence of the second more itinerant band is responsible for the electron transfer between the Hubbard subbands.

The next question to ask is where doped holes go in the quarter-filled system. Previously, we have shown [36] that three regimes emerge in increased screening, as discussed below. The reduction of the Coulomb interaction to $U_d = 4.0$ eV is sufficient to cause the loss of long-range AFM order in the $x^2 - y^2$ orbital due to reduced electron filling.

3.2. One-particle spectral density

First, in the weakly screened Mott insulator and for large U_d, the ground state is AFM, and holes naturally enter only the $x^2 - y^2$ orbital. In contrast, the second regime is found at intermediate screening [$\alpha \simeq 0.5$] or for interactions that are reduced from the outset (see Fig. 2b). Finally, in the third regime of strong screening ($\alpha \simeq 0.2$), hole doping occurs again into the $x^2 - y^2$ orbital, with the s electrons remaining unaffected [36]. This behavior is presented in more detail later in the text.

The different behavior in the three regimes mentioned in Sect. 3.1 is also reflected in the single-particle spectra shown in Fig. 3. Filling corresponds to doping with two holes, and twisted boundary conditions (TBC) are used to resolve more momenta [37–39]. Both for very strong $U_d = 8.0$ eV (see Fig. 3a) and for moderate $U_d = 4.0$ eV (see Fig. 4a), the correlations induce a gap in the x^2-y^2 band [40]. The lowest (occupied) states for electrons are in the s band at reduced $U_d = 4$ eV, i.e., both bands are partially filled. This can be seen in Fig. 2b, where we show the density of states for eight electrons (i.e., at quarter filling). Data were obtained by means of twisted boundary conditions (TBC), integrating over five sets of boundary conditions.

At strong screening when $\alpha = 0.2$, the occupied states in the $x^2 - y^2$ band are rather similar for $U_d = 8.0$ eV and $U_d = 4.0$ eV, except that the

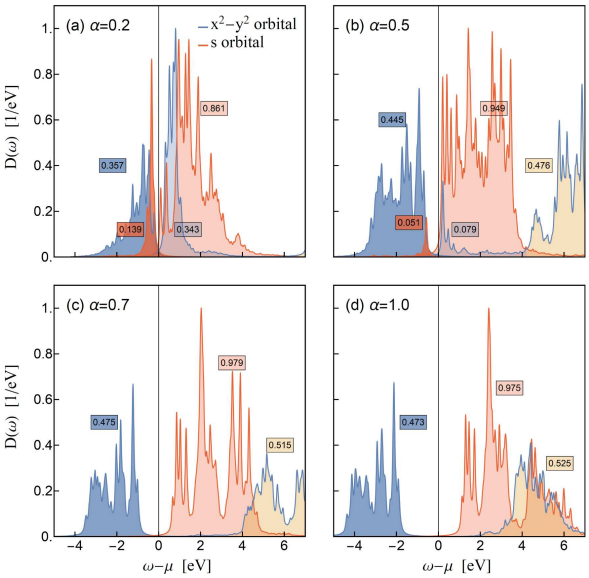

Fig. 3. Density of states $D(\omega)$ of undoped nickelate for $U_d = 8.0$ eV and for different values of screening α.

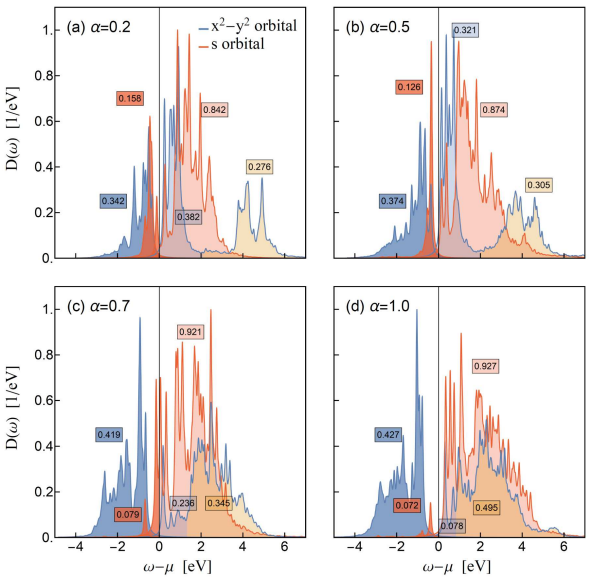

Fig. 4. Density of states $D(\omega)$ of undoped nickelate for $U_d = 4.0$ eV and for different values of screening α.

curvature of the occupied states changes along the $(\pi, 0) - (0, \pi)$ line. Also, the values of n_s and of the weight transferred to LHB are similar. Since this implies that interactions U' and J_H between d and s states do not play here a significant role, it supports the notion of a correlated (and doped) d band that is only affected by a metallic s band via self-doping.

In contrast, for stronger correlations, i.e., weaker screening $\alpha \in [0.5, 0.7]$, the spectra shown in Fig. 3b and c are affected by U_d. All electrons are here in the correlated x^2-y^2 states. It is remarkable

TABLE I

Electron densities n_d and n_s per spin obtained in the undoped nickelate for screened interactions ($\alpha < 1$). The weight of LHB $w_{\rm LHB}$ is increased by the kinetic weight transfer from UHB [41, 42].

U_d [eV]	α	n_d	n_s	$w^{>}_{\rm LHB}$	$w_{\rm LHB}$
8.0	0.20	0.358	0.139	0.343	0.700
	0.50	0.445	0.051	0.079	0.524
	0.70	0.475	0.021	0.011	0.485
	1.00	0.473	0.025	0.002	0.475
4.0	0.20	0.342	0.158	0.382	0.724
	0.50	0.374	0.126	0.321	0.695
	0.70	0.419	0.079	0.236	0.656
	1.00	0.427	0.072	0.078	0.505

that the occupied states fall almost at the same energies, independently of whether $U_d = 8.0$ eV or $U_d = 4.0$ eV (cf. Figs. 3 and 4). However, splitting between d and s states is clearly affected by U_d (via U' and J_H), which indicates that the s- and d-bands are in this regime directly coupled, not only via self-doping.

Analogous conclusions can be drawn from the fact that the undoped densities of states shown in Figs. 3(a) and 4(a) are extremely similar, i.e., in the regime of strong screening, both bands are partly filled, and the results hardly depend on U_d at all. In the intermediate regime, on the other hand, both bands are likewise partially filled. A comparison between Figs. 3 and 4 indicates that the s states close to the Fermi level could be doped away. In this regime, results depend on U_d, indicating that correlations are here more important to describe low-energy features close to the Fermi level.

Interestingly, the screening increases the density of s electrons, and simultaneously the density in the correlated band n_d decreases, as in the undoped case, the constraint $n_d + n_s = 1$ is satisfied. This makes LHB less than half-filled, and considerable spectral weight is transferred from UHB to the unoccupied part of LHB (i.e., above the Fermi energy μ). The mechanism of such a spectral weight transfer is well known in the partly filled Hubbard model [27, 28] and explains why the weight of LHB eventually exceeds 0.5 per spin. Here, doping in the Mott insulator is mimicked by the partial filling of the s band. The largest transfer of spectral weight is found at $U_d = 4.0$ eV and $\alpha = 0.2$ (see Table I). UHB forms only in the correlated x^2-y^2 band, and Hubbard subbands are absent within the s band even at $U_d = 8.0$ eV.

The regimes of weak and strong screening differ qualitatively. The number of correlated electrons n_d is close to $n_d = 0.5$ for weak screening but decreases rapidly for large screening. As a result, the total weight in LHB $w_{\rm LHB}$ increases somewhat above 0.7 for both $U_d = 8.0$ and $U_d = 4.0$, and the transferred weight is large (see Table I). The condition to

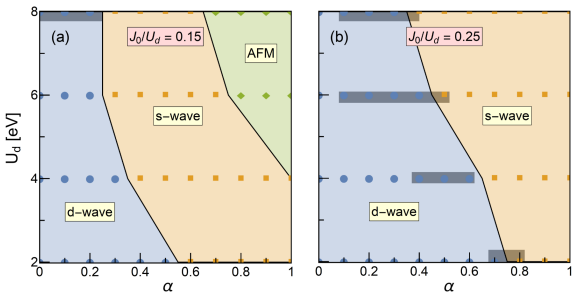

Fig. 5. Phase diagram in (U_d, α) plane for increasing Hund's exchange, i.e., increasing ratio J_0/U_d: (a) $J_0/U_d = 0.15$, and (b) $J_0/U_d = 0.25$. Antiferromagnetism (AFM) is found only in (a) for $J_0/U_d = 0.15$ and $U_d > 4$ eV The pairing has s- and d-wave symmetry, depending on the parameters. Tendency towards triplet pairing is highlighted by gray boxes; the points mark the parameters, at which the calculations were performed.

activate spectral weight transfer between the Hubbard subbands is finite hole doping in LHB of the correlated d band. Indeed, this hole doping nnd finite density within the s orbitals induces the spectral transfer towards LHB in the correlated band.

Altogether, the densities of states $D(\omega)$ give a metallic regime for intermediate ($\alpha = 0.5$) and strong ($\alpha = 0.2$) screening of strongly correlated $x^2 - y^2$ states (see Fig. 3). A large gap between the Hubbard subbands opens when $U_d = 8$ eV; this gap is reduced to ~ 0.5 eV when $U_d = 4.0$ eV. Nevertheless, the system still has an insulating gap that separates the Hubbard subbands. The electronic structure for the $x^2 - y^2$ band is typical for a doped Mott insulator, with the weight of UHB reduced by the kinetic processes in a doped system [41, 42]. Indeed, the weight in LHB above the Fermi energy increases by $\sim 2\delta$, where δ stands for the doping of LHB, which would also be the weight transferred from UHB to LHB by finite doping. In this regime, the s band is only weakly correlated, and Hubbard subbands are poorly visible.

3.3. Superconductivity in the two-band model

Finally, we investigate the nature of the SC state. Therefore, we first compute the ground state of the undoped two-band model on a finite square cluster, i.e., for 8 electrons on an 8-site cluster via exact (Lanczos) diagonalization. Next, the above cluster model is doped by 2 holes (by removing 2 electrons), and we look again at its ground state. After that, pairing operators (for s- or d-wave) are applied on the undoped ground state, and the overlap between the two states is obtained. We consider SC states of both symmetries by changing the Coulomb interaction U_d and the screening α in Fig. 5.

For strong and unscreened Coulomb repulsion $U_d > 4.0$ eV and weak Hund's exchange coupling (see Fig. 5a), one finds AFM order in the undoped system with no sign of pairing. This regime resembles the state of cuprates: the s-like band is empty, while the strongly correlated $x^2 - y^2$ band is half-filled and Mott insulating (see Fig. 2). This changes for weaker correlations (intermediate screening), where AFM order disappears and is replaced by s-wave pairing (see Fig. 5b).

The presence of d-wave pairing known from cuprates requires strong screening. In the regime of strong screening, doped holes enter the $x^2 - y^2$ band, and the model becomes similar to the cuprate model. Altogether, Fig. 5 tells that stronger Hund's exchange promotes triplet pairing, reduces effective correlations, and suppresses AFM order.

In the phase diagram in Fig. 5a, AFM phase and s-wave or d-wave pairings are accompanied by some indications of triplet pairing. As expected, the latter is more pronounced at stronger Hund's exchange coupling (see Fig. 5b). Energies obtained for the doping with either one $\uparrow$ or one $\downarrow$ hole are here degenerate with the energies obtained with two $\uparrow$ holes, indicating that the doped hole-pair is a triplet. In order to check the stability of this result, we used TBC again. The degeneracy is then lifted, and the $S^z = 0$ state has lower energy, suggesting that triplet pairing might be a finite-size effect. Finally, we remark that interaction screening reduces the stability of AFM order in the correlated band and broadens the range of stability of s-wave and d-wave pairings (see Fig. 5). Moreover, the needed Hund's exchange to stabilize d-wave pairing in a broad regime is rather large ($J_0/U_d \gtrsim 0.25$).

4. Conclusions

In summary, we have used exact diagonalization to investigate an effective two-band model for infinite-layer nickelates, where the band with a strong Ni($d_{x^2-y^2}$) character can be expected to be more correlated than the one with a rather extended s-like wave function of mostly rare-earth character. We focused here on the interactions in both bands, especially their relative strength, which also tunes the interorbital interactions between the two orbitals [20]. The latter give interband interactions and could generate superconducting pairing.

We have established that both the very strongly correlated and the strongly screened regimes support the mapping of the two-band model onto a single Hubbard-like band. For (unrealistically) strong interaction U_d, we find an antiferromagnetic Mott insulator without tendencies to superconductivity. In the more realistic screened regime, the s-like band takes up some of the charge carriers, and the states from both bands contribute to the Fermi energy. In this way, the correlated $x^2 - y^2$ band [17] is partly filled, and the spectral weight may be transferred to the unoccupied part of the lower Hubbard band [41].

For intermediate screening, the model is very rich, and the s-band hosts the doped holes forming s-wave pairs. We point out that this situation broadly corresponds to a Kondo-lattice-like scenario, with the caveat that the 'localized' $d_{x^2-y^2}$ spins can also move [4, 43, 44]. Hund's exchange coupling naturally yields ferromagnetic interaction between itinerant s carriers and $d_{x^2-y^2}$ spins, but it is interesting to note that s-wave pairing at stronger coupling was also obtained in a similar effective model with AFM spin-spin coupling [44]. Altogether, this shows that the model investigated here is very rich and predicts the pairing of different symmetry.

Acknowledgments

We thank Wojciech Brzezicki and Andres Greco for very insightful discussions. T. Plienbumrung acknowledges Development and Promotion of Science and Technology Talents Project (DPST). A.M. Oleś acknowledges Narodowe Centrum Nauki (NCN, Poland) Project No. 2021/43/B/ST3/02166 and is grateful for support via the Alexander von Humboldt Foundation Fellowship (Humboldt-Forschungspreis).

References

[1] D. Li, K. Lee, B.Y. Wang, M. Osada, S. Crossley, H.R. Lee, *Nature* **572**, 624 (2019).

[2] M. Jiang, M. Berciu, G.A. Sawatzky, *Phys. Rev. Lett.* **124**, 207004 (2020).

[3] T. Plienbumrung, M. Daghofer, A.M. Oleś, *Phys. Rev. B* **103**, 104513 (2021).

[4] M. Hepting, D. Li, C.J. Jia et al., *Nat. Mater.* **19**, 381 (2020).

[5] H. Lu, M. Rossi, A. Nag et al., *Science* **373**, 213 (2021).

[6] J.Q. Lin, P. Villar Arribi, G. Fabbris et al., *Phys. Rev. Lett.* **126**, 087001 (2021).

[7] L.-H. Hu, C. Wu, *Phys. Rev. Res.* **1**, 032046 (2019).

[8] Y.-H. Zhang, A. Vishwanath, *Phys. Rev. Res.* **2**, 023112 (2020).

[9] P. Jiang, L. Si, Z. Liao, Z. Zhong, *Phys. Rev. B* **100**, 201106 (2019).

[10] L. Si, W. Xiao, J. Kaufmann, J.M. Tomczak, Y. Lu, Z. Zhong, K. Held, *Phys. Rev. Lett.* **124**, 166402 (2020).

[11] X. Wu, D. Di Sante, T. Schwemmer, W. Hanke, H.Y. Hwang, S. Raghu, R. Thomale, *Phys. Rev. B* **101**, 060504 (2020).

[12] M. Klett, T. Schwemmer, S. Wolf et al., *Phys. Rev. B* **104**, L100502 (2021).

[13] R. Zhang, C. Lane, B. Singh, J. Nokelainen, B. Barbiellini, R.S. Markiewicz, A. Bansil, J. Sun, *Commun. Phys.* **4**, 118 (2021).

[14] E. Been, W.-S. Lee, H.Y. Hwang, Y. Cui, J. Zaanen, T. Devereaux, B. Moritz, C. Jia, *Phys. Rev. X* **11**, 011050 (2021).

[15] K. Higashi, M. Winder, J. Kuneš, A. Hariki, *Phys. Rev. X* **11**, 041009 (2021).

[16] A.S. Botana, K.-W. Lee, M.R. Norman, V. Pardo, W.E. Pickett, *Front. Phys.* **9**, 813532 (2021).

[17] M. Kitatani, L. Si, R. Arita, Z. Zhong, K. Held, *npj Quantum Mat.* **5**, 59 (2020).

[18] A. Kreisel, B.M. Andersen, A.T. Rømer, I.M. Eremin, F. Lechermann, *Phys. Rev. Lett.* **129**, 077002 (2022).

[19] Y. Nomura, M. Hirayama, T. Tadano, Y. Yoshimoto, K. Nakamura, R. Arita, *Phys. Rev. B* **100**, 205138 (2019).

[20] P. Adhikary, S. Bandyopadhyay, T. Das, I. Dasgupta, T. Saha-Dasgupta, *Phys. Rev. B* **102**, 100501 (2020).

[21] Y. Gu, S. Zhu, X. Wang, J. Hu, H. Chen, *Commun. Phys.* **3**, 84 (2020).

[22] F. Lechermann, *Phys. Rev. X* **10**, 041002 (2020).

[23] T.Y. Xie, Z. Liu, C. Cao, Z.F. Wang, J.L. Yang, W. Zhu, *Phys. Rev. B* **106**, 035111 (2022).

[24] A.M. Oleś, K. Wohlfeld, G. Khaliullin, *Condens. Matter* **4**, 46 (2019).

[25] A.S. Botana, M.R. Norman, *Phys. Rev. X* **10**, 011024 (2020).

[26] J.I. Budnick, B. Chamberland, D.P. Yang, C. Niedermayer, A. Golnik, E. Recknagel, M. Rossmanith, A. Weidinger, *Europhys. Lett.* **5**, 651 (1988).

[27] H. Eskes, M.B.J. Meinders, G.A. Sawatzky, *Phys. Rev. Lett.* **67**, 1035 (1991).

[28] M.B.J. Meinders, H. Eskes, G.A. Sawatzky, *Phys. Rev. B* **48**, 3916 (1993).

[29] P. Giannozzi, S. Baroni, N. Bonini et al., *J. Phys. Condens. Matter* **21**, 395502 (2009).

[30] P. Giannozzi, O. Andreussi, T. Brumme et al., *J. Phys. Condens. Matter* **29**, 465901 (2017).

[31] P. Giannozzi, O. Baseggio, P. Bonf'a et al., *J. Chem. Phys.* **152**, 154105 (2020).

[32] A. Dal Corso, *Comput. Mater. Sci.* **95**, 337 (2014).

[33] T. Plienbumrung, M. Daghofer, M.T. Schmid, A.M. Oleś, *Phys. Rev. B* **106**, 134504 (2022).

[34] G. Pizzi, V. Vitale, R. Arita et al., *J. Phys. Condens. Matter* **32**, 165902 (2020).

[35] J.B. Grant, A.K. McMahan, *Phys. Rev. B* **46**, 8440 (1992).

[36] T. Plienbumrung, M.T. Schmidt, M. Daghofer, A.M. Oleś, *Condens. Matter* **6**, 33 (2021).

[37] M. Shiroishi, M. Wadati, *Jpn. Phys. Soc.* **66**, 2288 (1997).

[38] D. Poilblanc, *Phys. Rev. B* **44**, 9562 (1991).

[39] W.-G. Yin, W. Ku, *Phys. Rev. B* **80**, 180402 (2009).

[40] F. Lechermann, *Phys. Rev. B* **101**, 081110 (2020).

[41] H. Eskes, A.M. Oleś, *Phys. Rev. Lett.* **73**, 1279 (1994).

[42] H. Eskes, A.M. Oleś, M.B.J. Meinders, W. Stephan, *Phys. Rev. B* **50**, 17980 (1994).

[43] G.-M. Zhang, Y.-F. Yang, F.-C. Zhang, *Phys. Rev. B* **101**, 020501 (2020).

[44] Z. Wang, G.-M. Zhang, Y.-F. Yang, F.-C. Zhang, *Phys. Rev. B* **102**, 220501 (2020).